RESEARCH PAPER



Surface modification strategy based on the conjugation of NaYF₄:5% Eu luminescent nanoprobe with organic aromatic compounds for application in bioimaging assays

Rodrigo da Silva Viana • Luciana Amaral de Mascena Costa • Andressa N. R. Leal • Tyrslai M. Williams • Liquian Luan • Guanyu Zhang • Maodie Wang • Ashlyn C. Harmon • Janaina V. dos Anjos • Rafael Cueto • Manoel Adrião Gomes Filho • Eduardo H. L. Falcão • Maria G. H. Vicente • Severino A. Junior • J. Michael Mathis

Received: 29 May 2018 / Accepted: 19 November 2018 / Published online: 23 January 2019 © Springer Nature B.V. 2019

Abstract Colon cancer is one of the world's most deadly diseases. Because of its internal location, it is necessary to obtain faster and more efficient diagnostic tools for this organ site. In this context, we studied the development of new luminescent nanoprobes (LNPs) as an alternative diagnostic apparatus for detecting this disease. The nanoparticles examined herein are

Electronic supplementary material The online version of this article (https://doi.org/10.1007/s11051-018-4422-0) contains supplementary material, which is available to authorized users.

R. da Silva Viana · A. N. R. Leal · J. V. dos Anjos · E. H. L. Falcão · S. A. Junior (ﷺ)
Department of Fundamental Chemistry, Federal University of Pernambuco, Av. Prof. Moraes Rego, 1235 - Cidade Universitária, Recife, Pernambuco 50670-901, Brazil e-mail: salvesjr@ufpe.br

L. A. de Mascena Costa · M. A. G. Filho Department of Animal Morphology and Physiology, Federal Rural University of Pernambuco, Rua Manuel de Medeiros, s/n – Dois irmãos, Recife, Pernambuco 52171-900, Brazil

T. M. Williams · L. Luan · G. Zhang · M. Wang · R. Cueto · M. G. H. Vicente
Department of Chemistry, Louisiana State University, Baton Rouge, LA 70803, USA

A. C. Harmon · J. Mathis (⋈)
Department of Comparative Biomedical Sciences, School of Veterinary Medicine, Louisiana State University, 1909 Skip Bertman Drive, Baton Rouge, LA 70803, USA e-mail: jmathis@lsu.edu

lanthanide-doped sodium yttrium fluoride (NaYF₄:Ln) and have shown to be promising as investigative devices. However, significant problems with the use of LNPs are the lack of biocompatibility and the targeting of the system to tumor regions. One of the strategies to bypass these problems is to increase of the particle lipophilicity modifying their surfaces with organic compounds that present high similarity to the biological system. In this work, we synthesized six new materials for use in bioimaging techniques obtained from the combination of nanoparticles of NaYF₄:5%Eu with organic aromatic compounds covalently bonded. The materials were characterized structurally and morphologically using XRD and TEM, techniques, which showed the identification of the crystallographic phase β -NaYF₄:5%Eu and its nanometric size (particles smaller than 50 nm). The conjugation process was confirmed by FT-IR spectra analysis and from the TGA profile. Excitation and emission spectra allowed the evaluation of the optical properties of the synthesized compounds. The interaction and cellular uptake was confirmed when HT-29 colon cancer cells were exposed to LNPs, indicating that the developed system has promising applications in bioimaging procedures.

Keywords Luminescent nanoprobe · Surface conjugation · Couple reaction · Cell imaging · NaYF₄:5%Eu · Diagnostic tool



23 Page 2 of 15 J Nanopart Res (2019) 21: 23

Introduction

Colon cancer is the fourth most common cancer in the world and ranks second in cancer mortality in the USA (Siegel et al. 2017). Currently, colon cancer detection protocols rely on the use of colonoscopy, a method used to identify nascent tumor formation. Like many cancers, diagnosis at an early stage significantly increases the chances of cure. However, as this disease has few overt signs or symptoms, in most cases colon cancer is detected at advanced stages, resulting in a poor prognosis (Arnold et al. 2017). Therefore, the development of new clinical diagnostic tools is necessary to increase colon cancer survival rates. The search for different diagnostic approaches has motivated our efforts for the development of new materials that may serve as alternative probes for investigative devices. Among these, luminescent nanoprobes (LNPs) typically present with chemical stability, high quantum emission efficiency, and low toxicity in a biological environment, resulting in properties that are distinct from classically used materials such as organic dyes (Kim and Cho 2015).

There are several kinds of LNPs with potential application for bioimaging, from traditional luminescent inorganic materials such as quantum dots (Karakoti et al. 2015; Hildebrandt et al. 2017) to luminescent carbonaceous nanocompounds (C-dots) (Luo et al. 2013; do D'Angelis et al. 2015). Among these, the lanthanidedoped sodium yttrium fluoride (NaYF₄:Ln³⁺) nanoparticles are a class of very promising LNPs, due to their unique spectroscopic properties such as photostability, low phonon frequency, narrow and well-defined emission lines, wide Stokes/Anti-Stokes displacement (< 200 nm), and long lifetimes (> 10^{-4} s). Among the lanthanides, the Eu3+ ion is notable for having intense and predominant emission lines in the red region, because it is easily introduced into inorganic matrices and forms systems that work very well as a probe for biochemical or biological applications (Binnemans 2015). These properties have been exploited through their use in both in vivo and in vitro biological imaging assays (Blasse and Grabmaier 1994; Bünzli and Piguet 2005; Binnemans 2015). Some examples of NaYF₄-like materials that exploited Lanthanide ion-based luminescence properties are reported in the literature, as described in the work of (Sojka et al. 2016), which utilized a strategy for the synthesis of Lectin conjugated with NaGdF₄:Eu³⁺ to create luminescence nanoparticles for tumor imaging in vivo. The authors determined the specificity of the nanoparticles for targeting melanoma, which was determined by luminescence microscopy.

One of the critical factors that qualify LNPs as promising agents for bioimaging techniques is the effectiveness of their interaction with the biological medium. However, to entirely achieve this goal, it is necessary to increase the degree of lipophilicity on the surface of the material (Veber et al. 2002; Waring 2010). A possible method to achieve this increase is to bind them covalently with organic compounds. Oluwole et al. (2016) reported the use of nanoparticles of SiO₂ and ZnO/SiO₂ conjugated to zinc monocarboxyphenoxy phthalocyanine for photophysical studies. Using in vitro assays, the authors showed good cellular interaction after the surface modification, indicative of a promising system for use in photodynamic therapy. Another example concerning the conjugation of organic molecules for biomedical applications was the synthesis of chitosan nanoparticles covalently attached to the organic fluorescent molecule BODIPY (Bor et al. 2017). This system was revealed to have good viability and fluorescence, suggesting its utilization for biological imaging assays.

In the present work, we report the production of six new LNPs based on the combination of europium-doped sodium yttrium fluoride (NaYF₄:5%Eu) nanoparticles linked to p-Coumaric acid, tyrosine, BODIPY, and zinc phthalocyanine (ZnPc) using a surface modification strategy. We also provide an evaluation of their interaction with the HT-29 colon cancer cell line and investigate their potential use as bioimaging diagnostic tools using in vitro assays.

Materials and methods

Materials

The compounds 10-(2-carboxyethyl)-5,5-difluoro-5H-dipyrrolo[1,2-c:2',1'-f][1,3,2]diazaborinin-4-ium-5-uide (BODIPY COOH), 5,5-diisothiocyanato-1,3,7,9-tetramethyl-10-phenyl-5H dipyrrolo[1,2:2',1'f][1,3,2]diazaborinin-4-ium-5-uide (BODIPY NCS), Zinc phthalocyanine (ZnPc) was prepared according to the procedure reported in the supplementary information. Europium and yttrium oxide (99%), octadec-1-ene (90%), Tetraethoxysilane (98%; TEOS), (Trimethylsilyl)isothiocyanate (99%; TMSNCS), 3-Triethoxysilylpropylamine (\geq 98%; APTES), oleic acid (99%), sodium hydroxide (\geq 98%; NaOH), ammonium



fluoride (\geq 98%; NH₄F) and 2-(1H-Benzotriazole-1-yl)-1,1,3,3-tetramethylaminium tetrafluoroborate (\geq 97%; TBTU), p-Coumaric acid (\geq 98%), N-(9-Fluorenylmethoxycarbonyl)-O-tert-butyl-L-tyrosine (\geq 98%; Fmoc-Tyr(tBu)-OH), and tin chloride were obtained from Sigma-Aldrich (St. Louis, MO). The chemicals hydrochloric acid, dimethylformamide (DMF), methanol, toluene, acetone, and cyclohexane were purchased from VWR International (Radnor, PA). Yttrium and Europium oxides were used as received to prepare the corresponding lanthanide chlorides by treatment with concentrated HCl (35%).

Synthesis procedures

Synthesis of the europium-doped sodium yttrium fluoride nanoparticles (NaYF₄:5%Eu) This methodology was adapted from Johnson et al. (2011). In a round bottom flask was added 0.95 mmol of YCl3·6H2O, 0.05 mmol of EuCl3·6H2O, 4 mL of oleic acid, and 15 mL of octadecene, and the entire system was heated for 30 min at 140 °C under a nitrogen atmosphere, whereupon a yellow solution was formed. Subsequently, the system was cooled and a mixture formed of 2.5 mmol NaOH, and 4 mmol NH4F in 10 mL methanol was prepared and added to the flask. The flask was stirred for 15 h under nitrogen atmosphere. Afterward, the flask was heated at 70 °C for 5 min, and the solution became dark. Finally, the flask was heated rapidly to the temperature of 280 °C for 90 min. The contents of the flask were collected at room temperature, and the particles produced were precipitated using methanol. The product was centrifuged, separated, and washed five times with toluene using successive centrifugation for 15 min at 8000 rpm.

Synthesis of the europium-doped sodium yttrium fluoride nanoparticles amino functionalized (NaYF₄:5%Eu-NH₂) Functionalization of the amine functional groups was based on the use of the sol-gel Stöber methodology (Stöber et al. 1968) adapted from the work described by Liu et al. (2014). For this synthesis, 20 mg of NaYF₄:5%Eu was dispersed in 30 mL of cyclohexane in an ultrasonic bath for 1 h in an Erlenmeyer flask. After that, 7.50 mL of ultrapure water, 8.94 mL of NH₄OH, and 54 μL of Tetraethoxysilane (TEOS) were added, and the system was maintained under vigorous stirring for 4 h. Finally, 26 μL of 3-Triethoxysilylpropylamine (APTES) was added, and

the system remained under stirring for an additional 1 h. The product obtained is removed as a white solid by centrifugation at 8000 rpm for 15 min, washed successively by centrifugations (five washes using a 1:1 ethanol/water solution), and dried under vacuum.

Conjugation procedures

Modification of the NaYF₄:5%Eu-NH₂ surface with p-Coumaric acid The first step included the introduction of a p-Coumaric acid portion into the NaYF₄:5%Eu-NH₂ nanoparticles using an amidification methodology. In this reaction, the nanoparticles containing a free amino moiety (10 mg), 3-(4-acetoxyphenyl)acrylic acid (1.5 mmol) were activated with N,N,N',N'-tetramethyl-O-(benzotriazol-1yl)uronium tetrafluoroborate (TBTU; 1.5 mmol) in a mixed of DMF (5 mL) and Triethylamine (5 mL), both dry. The mixture was allowed to react for 24 h under an inert atmosphere. After this period, the reaction contents were centrifuged, separated, and washed five times with DMF (5 mL each) using successive centrifugation cycles for 15 min at 8000 rpm, producing NaYF₄:5%Eu-Coumaric acid particles. The second step consisted of the acetyl group removal present in the particles. In this procedure, NaYF₄:5%Eu-NH₂ nanoparticles (5 mg) were added to a mixture of LiOH (10.5 mg), distilled water (2.5 mL), methanol (2.5 mL), and THF (2.5 mL), and the mixture was maintained for 24 h at room temperature under stirring conditions. After that, 1 M HCl was added dropwise until a pH 5.0 was achieved. The particles were centrifuged again, separated, and washed five times with water (5 mL each) using successive centrifugation cycles for 15 min at 8000 rpm, producing NaYF₄:5%Eu-Coumaric particles.

Modification of the NaYF₄:5%Eu-NH₂ surface with tyrosine The first step included the introduction of a tyrosine residue on NaYF₄:5%Eu-NH₂ nanoparticles using an amidification methodology. The reaction involved the conjugation of the amino nanoparticles with Fmoc-O-tert-butyl-L-tyrosine (1.5 mmol) under activation with N,N,N',N'-tetramethyl-O-(benzotriazol-1-yl)uronium tetrafluoroborate (TBTU; 1.5 mmol) in a mixture of DMF (5 mL) and triethylamine (5 mL), both dry. The mixture was maintained under stirring for 24 h and under an inert atmosphere. The resulting particles were centrifuged, separated, and washed five times with water (5 mL each) using successive centrifugation cycles for 15 min at 8000 rpm, producing NaYF₄:5%Eu-

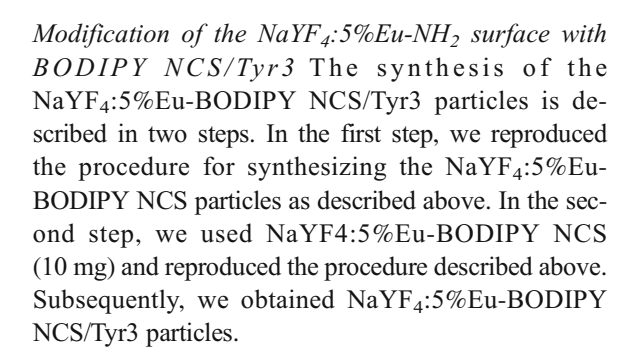


23 Page 4 of 15 J Nanopart Res (2019) 21: 23

Tyr1. The second step consisted of the removal of the Fmoc group present in the particles. Then, NaYF₄:5%Eu-Tyr1 (5 mg) were dissolved in 5 mL of piperidine:DMF (8:2, v/v) and maintained for 24 h at room temperature under stirring conditions. The particles were centrifuged again, separated, and washed five times with DMF (5 mL each) using successive centrifugation cycles for 15 min at 8000 rpm, producing NaYF₄:5%Eu-Tyr2. The third step removed the tertbutyl group on the particles. The NaYF₄:5%Eu-Tyr2 nanoparticles (5 mg) were dissolved in a mixture of LiOH (10.5 mg), distilled water (2.5 mL), methanol (2.5 mL), and THF (2.5 mL) and maintained for 24 h at room temperature under stirring conditions. After that, 1 M HCl was added dropwise until a pH 5.0 was achieved. The particles were centrifuged, separated, and washed five times with water (5 mL each) using successive centrifugation cycles for 15 min at 8000 rpm, producing NaYF₄:5%Eu-Tyr3.

Modification of the NaYF₄:5%Eu-NH₂ surface with BODIPY COOH To obtain NaYF₄:5%Eu-BODIPY COOH nanoparticles, a coupling reaction between 10-(2-carboxyethyl)-5,5-difluoro-5H-dipyrrolo[1,2-c:2',1'-f][1,3,2]diazaborinin-4-ium-5-uide (BODIPY COOH; 1.5 mmol) and NaYF₄:5%Eu-NH₂ nanoparticles (10 mg) was performed using as activation agent the N,N,N',N'-tetramethyl-O-(benzotriazol-1-yl)uronium tetrafluoroborate (TBTU; 1.5 mmol) in a mixture of DMF (5 mL) and triethylamine (5 mL), both dry. The mixture was allowed to react for 24 h under an inert atmosphere. The resulting particles were centrifuged, separated, and washed five times with DMF (5 mL each) using successive centrifugation cycles for 15 min at 8000 rpm, producing NaYF₄:5%Eu-BODIPY COOH.

Modification of the NaYF₄:5%Eu-NH₂ surface with BODIPY NCS In order to obtain NaYF₄:5%Eu-BODIPY NCS nanoparticles via coupling reaction, 5,5-diisothiocyanato-1,3,7,9-tetramethyl-10-phenyl-5H dipyrrolo[1,2:2',1'f][1,3,2]diazaborinin-4-ium-5-uide (BODIPY NCS; 1.5 mmol) and NaYF₄:5%Eu-NH₂ nanoparticles (10 mg) were dissolved in dry acetone (5 mL). The mixture was allowed to react for 24 h at room temperature under an inert atmosphere. The resulting particles were centrifuged, separated, and washed five times with acetone (5 mL each) using successive centrifugation cycles for 15 min at 8000 rpm, producing NaYF₄:5%Eu-BODIPY NCS.



Modification of the NaYF₄:5%Eu-NH₂ surface with ZnPc To obtain NaYF₄:5%Eu-ZnPc nanoparticles through a coupling reaction, zinc phthalocyanine (ZnPc; 1.5 mmol) and NaYF₄:5%Eu-NH₂ nanoparticles (10 mg) were conjugated using as activation agent N,N,N',N'-tetramethyl-O-(benzotriazol-1-yl)uronium tetrafluoroborate (TBTU; 1.5 mmol) in a mixture of DMF (5 mL) and triethylamine (5 mL); the mixture was allowed to react for 24 h under an inert atmosphere. The resulting particles were centrifuged, separated, and washed five times with DMF (5 mL each) using successive centrifugation cycles for 15 min at 8000 rpm, producing NaYF₄:5%Eu-ZnPc.

Determination of the amount of organic compound added for modifying the particle surfaces

To rationalize the amount of the aromatic organic compounds used in the conjugation with LNPs, three different reaction conditions were evaluated. Optimization of the amount of conjugate was obtained as a function of the organic molar equivalent using p-coumaric acid and tyrosine, to the values equal to 0.18 mmol, 0.30 mmol, and 1.50 mmol combined with 10 mg of NaYF₄:5%Eu-NH₂. TGA analysis of the conjugate compounds (NaYF₄:5%Eu-Coumaric and NaYF₄:5%Eu-Tyrosine) revealed the amount of residual mass, which was directly proportional to the amount of conjugated organic compound (Table S1-S3). The analysis showed that the best condition was obtained with the use of 1.5 mmol of organic fraction, which provided higher conjugation percentages of organic molecules into the particles. From these data, this proportion was adopted for all the conjugation reactions presented in this work.

Cell culture and confocal microscopy

The human colon adenocarcinoma cell line HT-29 was obtained from the American Type Culture Collection



(Manassas, VA) and grown in Dulbecco's modified Eagle's medium (DMEM) supplemented with 10% fetal bovine serum, 50 U/mL penicillin, and 50 mg/mL streptomycin, under 5% CO₂ and 37 °C culture conditions. The cells were plated in 35 mm glass bottom cell culture dishes (Thermo Fisher Scientific; Waltham, MA) for confocal microscopy. After 24 h, the cells were treated with 100 μ g/mL of each LNPs for an additional 24 h. After this period, the media was removed, and the cells were incubated for 10 min with 1 mL of a phosphate buffered saline (PBS) solution containing 5 μ L of Hoechst 33342 dye. Subsequently, the cells were washed three times with 1 mL of PBS and visualized by confocal microscopy using a Leica SP8 confocal platform with a white light laser source.

XTT cytotoxicity assay

HT-29 cells were plated overnight in 96 well dishes at a concentration of 10,000 cells/well in 200 µL DMEM media described above under 5% CO₂ and 37 °C culture conditions. After this period, the media was removed and replaced with 200 µL media containing 1, 10, or 100 μg/mL of NaYF₄:5%Eu-NH₂. As controls, cells were untreated (PBS) or treated with 10 µg/mL doxorubicin. After 72 h treatment, cell viability was determined using an XTT assay (Scudiero et al. 1988). To each well was added 50 µL of XTT detection solution (Cell Signaling Technology; Danvers, MA), and after 2 h of incubation at 37 °C, the optical density of each well was measured at 450 nm using a Spectra Max 190 plate reader (Molecular Devices; Sunnyvale, CA). Wells containing no cells but containing the DMEM media and XTT reagent alone were used as blank readings. The data were analyzed and expressed as mean percent cell growth of control (untreated) cells to determine any effect on cell viability. Samples were assayed in replicates of eight.

Nanoparticle characterization

Powder X-ray diffraction (PXRD) data were recorded at room temperature on a PANalytical Empyrean XRD with Cu K α (λ = 1.5406 Å) radiation. Fourier transform infrared spectra (FT-IR) were measured on a Bruker spectrometer (model Tensor 27) at the range of 4000–650 cm⁻¹ equipped with a Pike single-bounce diamond/ZnSe ATR cell. The photoluminescence properties were investigated using a spectrofluorometer Fluorolog-3

(model FL3-22TAU3; Jobin-Yvon, Edison, NJ) with a continuous 450 W xenon lamp and UV xenon flash tube for excitation, double-grating monochromator in the excitation and UV-VIS (ultraviolet-visible) emission position. All optical data were obtained using particle suspensions in PBS (pH 7.4) at a concentration of $100~\mu g/ml$. In addition, the emission spectra were corrected for the wavelength dependent response of the detection system. A silicon photodiode reference detector was used to monitor and compensate for the variation in the xenon lamp output, using typical correction spectra provided by the manufacturer.

Results and discussion

Structural and microscopic evaluation

The structural characteristics of the compounds were evaluated using the X-ray diffraction powder (PXRD). We observed that NaYF₄:5%Eu showed good correlation with the simulated diffraction pattern (Tu et al. 2013). The results in Fig. 1 indicate that the synthesized compounds were obtained with high phase purity (red line) and were organized in the crystalline phase of β -NaYF₄ in the space group P-6 with hexagonal symmetry. This lanthanide compound was functionalized with -NH₂ terminal groups using the modified sol-gel Stöber route (Stöber et al. 1968; Liu et al. 2014). The structure of the compound of NaYF₄:5%Eu obtained after the

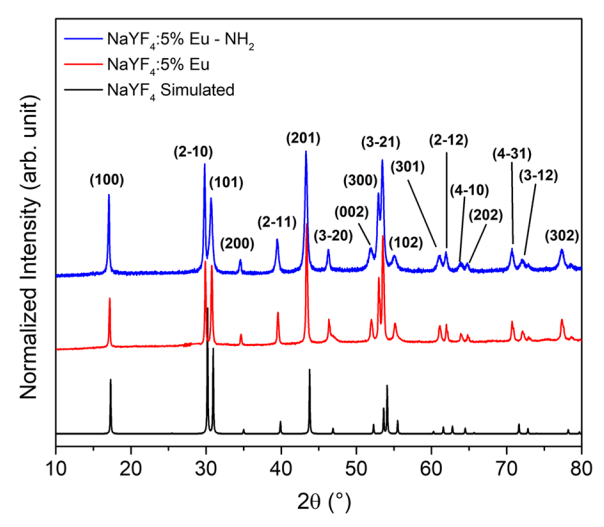


Fig. 1 Experimental PXRD patterns for NaYF₄:5%Eu (red line) NaYF₄:5%Eu-NH₂ (blue line) LNPs and NaYF₄ simulated pattern reported from reference (Tu et al. 2013) (black line)



23 Page 6 of 15 J Nanopart Res (2019) 21: 23

functionalization processes (NaYF₄:5%Eu-NH₂) is also shown in Fig. 1 (blue line). These results demonstrate the stable structure of the compounds after surface modification with amine groups and reveal the absence of impurities in the analyzed samples. The morphology of NaYF₄:5%Eu was evaluated using transmission electron microscopy (TEM), as shown in Fig. 2. TEM analysis for NaYF₄:5%Eu (Fig. 2a) shows the formation of nanoparticles smaller than 20 nm before the amino group functionalization. The same analysis for NaYF₄:5%Eu-NH₂ shows an increase in the particle size; the mean particle size was less than 50 nm and arranged as agglomerates (Fig. 2b). The nanometric dimension of the particles is in agreement with results previously reported in the literature (Zhou et al. 2011; Bhunia et al. 2013; Ansari and Yadav 2016; Syamchand and George 2016; Xu et al. 2016; Generalova et al. 2017; Wang et al. 2018), which supports its subsequent use in bioimaging assays.

Chemical and compositional analysis

The compound NaYF₄:5%Eu-NH₂ was used as a matrix for the functionalization with small aromatic molecules, with the aim of providing a better interaction between the nanoparticles and the surface of a target cell. It is known in the literature that an increase in the lipophilicity of species to be used as ligands in a biological medium should enhance the specificity in the interaction with cell surface targets (Waring 2010). Therefore, we selected six organic compounds well described in the literature with binding properties in biological systems to obtain the

following new conjugated nanoparticles: NaYF₄:5%Eu-Coumaric, NaYF₄:5%Eu-Tyr3, NaYF₄:5%Eu-BODIPY COOH, NaYF₄:5%Eu-BODIPY NCS, NaYF₄:5%Eu-BODIPY NCS, NaYF₄:5%Eu-ZnPc, and NaYF₄:5%Eu-BODIPY NCS/Tyr3. Figure 3 shows a representative diagram of the materials used in this work. It is important to note that the addition of organic compounds has already been reported in the literature as an interesting way to increase the specificity cellular and viability in the interaction between nanoparticles and tumor cells (Li et al. 2014). Therefore, in this work, we provide new alternatives for obtaining this class of materials.

Coupling reactions were used to produce most of the conjugated nanoparticles. They were performed in two steps using TBTU as the coupling agent for the amidification reaction (Valeur and Bradley 2009). This synthetic route was used for conjugation of the NaYF₄:5%Eu-Coumaric particles as shown in the scheme described in Fig. S3. This reaction was performed in two steps, in which the first step was the reaction between the 3-(4-acetoxyphenyl)acrylic acid (coumaric acid) and NaYF₄:5%Eu-NH₂ particles, yielding the intermediate compound NaYF4:5%Eu-Ac. Coumaric. The second step was the removal of the acetyl protecting group and generation of the hydroxyl group in the final compound, maintaining the organic structure of NaYF₄:5%Eu-Coumaric as close as possible to the p-Coumaric acid molecular structure.

The functionalization process of NaYF₄:5%Eu-NH₂ was analyzed by infrared spectroscopy (FT-IR), and a comparison was performed between NaYF₄:5%Eu (black line) and NaYF₄:5%Eu-NH₂ (red line) particles

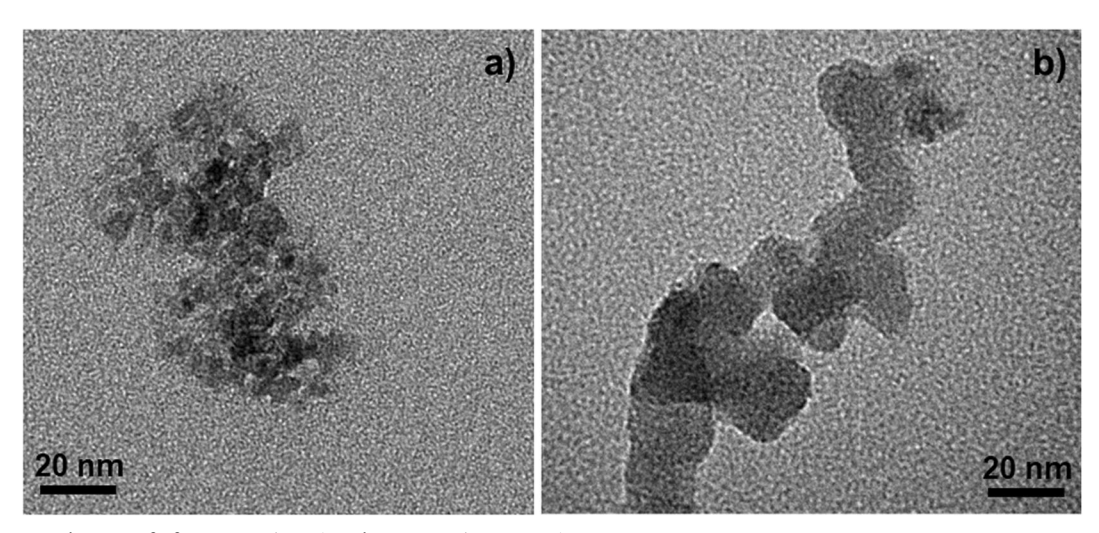


Fig. 2 TEM images of of NaYF₄:5%Eu a) and NaYF₄:5%Eu-NH₂ b) LNPs



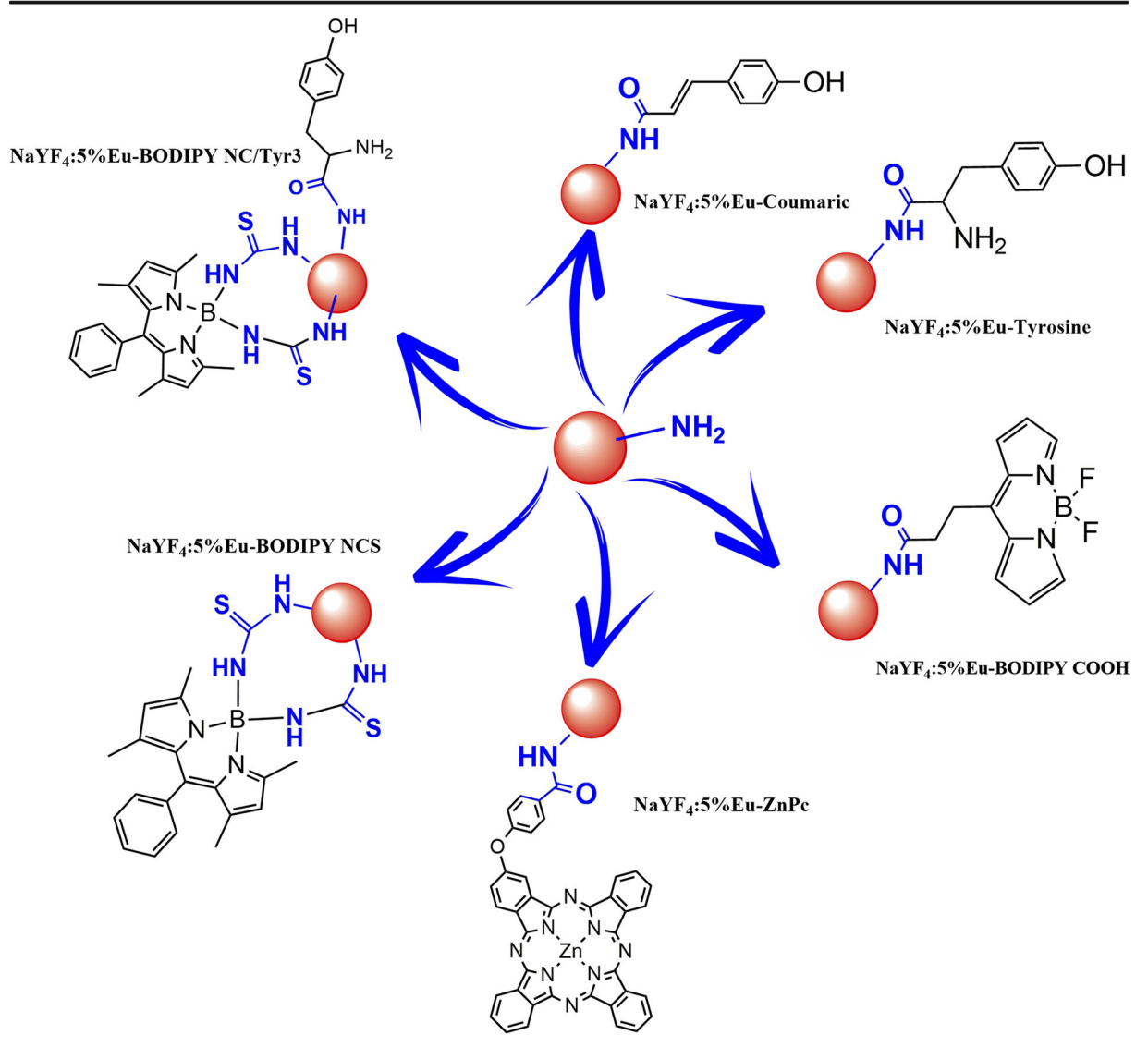


Fig. 3 Representation of the LNPs obtained by the conjugation reaction between the NaYF₄:5%Eu-NH₂ particles and the organic aromatic compounds investigated in this work

as shown in Fig. 4. The spectrum revealed the presence of a broad and strong band centered at 1070 cm⁻¹ on NaYF₄:5%Eu-NH₂ due to asymmetric Si-O-Si, which indicated the presence of silane groups in the particles. The functionalization of the amino groups was observed by the presence of bands located at 1635 cm⁻¹ and 794 cm⁻¹ due to the N-H stretches directed in the plane and outside it, respectively. It is important to notice that results described in the literature present an FT-IR profile similar to that found in the present study (Liu et al. 2014; Kostiv et al. 2015).

To analyze the preparation of NaYF₄:5%Eu-Coumaric particles, the materials obtained in the first

and second steps were characterized by FT-IR. A preliminary analysis (Fig. S4) shows the spectral profiles comparing NaYF₄:5%Eu-NH₂ (red line), NaYF₄:5%Eu-Ac. Coumaric (blue line), and NaYF₄:5%Eu-Coumaric (pink line). No apparent differences were observed, except for the region between 1800 and 1250 cm⁻¹. Figure S4 further shows a section of the spectrum, where the presence of an N-H stretch in 1635 cm⁻¹ was noted for NaYF₄:5%Eu-NH₂ (red line). The spectrum of the compound NaYF₄:5%Eu-NH₂-Ac. Coumaric shows a band at 1738 cm⁻¹, which was related to an ester carbonyl stretch, relative to the acetyl group of NaYF₄:5%Eu-NH₂-Ac. Coumaric (blue line).



23 Page 8 of 15 J Nanopart Res (2019) 21: 23

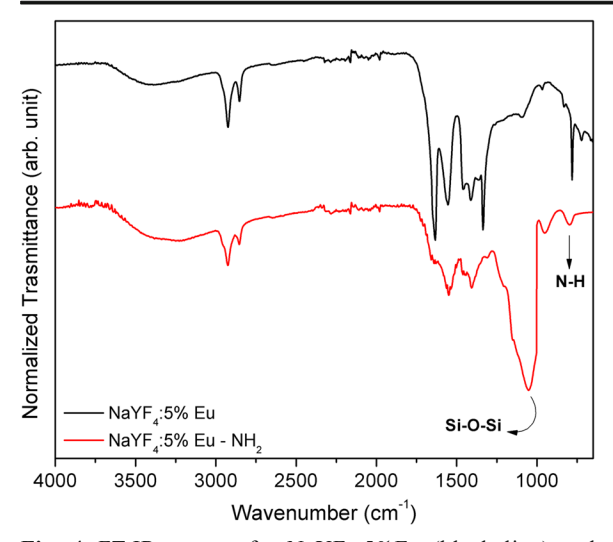
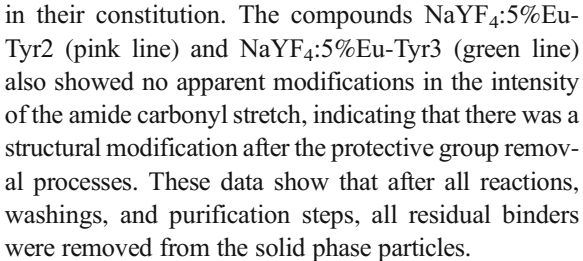


Fig. 4 FT-IR spectra for NaYF4:5%Eu (black line) and NaYF4:5%Eu-NH2 (red line)

In addition, a band centered at 1630 cm⁻¹ indicated the presence of C=O groups of the amide formed in the formation reaction of NaYF₄:5%Eu-Ac. Coumaric. The compound NaYF₄:5%Eu-Coumaric (red line) shows a less intense carbonyl band related to the ester group. Finally, the maintenance of the band for the C=O stretch of the amide group was maintained, indicating that the conjugated material was successfully obtained.

Conjugation reactions for the synthesis of NaYF₄:5%Eu-Tyr3 particles were performed as shown in Fig. S5. The reaction was carried out in three steps, where the first step was the coupling reaction between tyrosine and NaYF₄:5%Eu-NH₂, generating NaYF₄:5%Eu-Tyr1 as a product. The second step consisted of removing the first protective group in alkaline medium and NaYF₄:5%Eu-Tyr2 production. Finally, the desired compound NaYF₄:5%Eu-Tyr3 was obtained by removal of the last protecting group in an acid medium. The functionalization of the compound NaYF₄:5%Eu-NH₂ with compounds derived from tyrosine and evaluated using FT-IR, as shown in Fig. S6. A preliminary analysis showed that the spectral profiles of NaYF₄:5%Eu-NH₂ (red line), NaYF₄:5%Eu-Tyr1 (blue line), NaYF₄:5%Eu-Ty2 (pink line) and NaYF₄:5%Eu-Ty3 (pink line) did not undergo major changes, except for the region between 1800 and 1250 cm⁻¹. In the highlighted region, we observed the presence of the band for C=O amide stretch in the region of 1658 cm⁻¹ for NaYF₄:5%Eu-Tyr1 (blue line), indicating that the particles contained the organic moiety of interest



We used the same methodology, now performed as a single step, to carry out the conjugation of BODIPY molecules with terminal carboxylic acids (BODIPY COOH). The schematic diagram for this conjugation reaction is shown in Figure S7. The evaluation of organic moiety conjugation was performed using infrared spectroscopy (Fig. S8). FT-IR results showed slight changes in the spectra of NaYF₄:5%Eu-NH₂ (red line) and NaYF₄:5%Eu-BODIPY COOH (blue line) in the region of the formation of the amide bond, as demonstrated by the modification of the spectral profile at 1642 cm⁻¹ due to the C=O stretch of the amide group. We also used infrared spectroscopy to evaluate the conjugation of NaYF₄:5%Eu-NH₂ nanoparticles with BODIPY N=C=S terminal groups (BODIPY NCS). The schematic diagram for this conjugation reaction is shown in Fig. S9. We also provided a comparison among NaYF₄:5%Eu-NH₂ (red line), NaYF₄:5%Eu-BODIPY NCS (blue line) and BODIPY NCS free (pink line), as shown in Fig. S10. We would expect that, if the conjugation reaction did not occur or occurred partially (in only one of the -N=C=S groups), the band in BODIPY NCS centered at 2088 cm⁻¹ would be maintained in NaYF₄:5%Eu-BODIPY NCS (blue line). However, such a stretch did not appear in this region, indicating that there was a conjugation of BODIPY NCS with NaYF₄:5%Eu-NH₂.

To validate the conjugation of ZnPc with the nanoparticles of NaYF₄:5%Eu-NH₂, we used the same methodology for the coupling reactions performed in this work. The schematic diagram of the methodology employed is shown in Fig. S11. The conjugation reaction analysis was also performed using infrared spectroscopy (Fig. S12). The infrared graph reveals slight changes in the spectra of NaYF₄:5%Eu-NH₂ (red line) and NaYF₄:5%Eu-ZnPc (blue line) in the region of the amide bond formation, which was demonstrated by a spectral profile modification at 1642 cm⁻¹.

The last material obtained in this work was NaYF₄:5%Eu-BODIPY NCS/Tyr3, which was synthesized using the combination between the BODIPY NCS



and tyrosine conjugating procedures. A schematic diagram of the methodology employed is shown in Fig. S13. An analysis of the obtained compound was performed using FT-IR (Fig. S14). When comparing NaYF₄:5%Eu-NH₂ (red line) and NaYF₄:5%Eu-BODIPY NCS/Tyr3 (blue line), we observed the absence of the -N=C=S moiety, indicating that there is no free BODIPY NCS in the particles. In addition to these findings, we observed the presence of the C=O stretch of amide, indicating that a tyrosine residue integrates the final material.

Quantification of the organic residue in the LNPs was obtained using thermogravimetric analysis (TGA). Our evaluation protocol was based on the difference between the percentage of the residual mass of NaYF₄5%Eu-NH₂ and conjugated particles (Fig. 5). The particles based on p-Coumaric acid derivatives presented 59% of residual mass for NaYF₄:5%Eu-Ac. Coumaric and 63% for NaYF₄:5%Eu-Coumaric. The difference analysis for NaYF₄:5%Eu-Coumaric showed a Δ_{Residue} = 33% (Fig. 5a). For tyrosine-conjugated particles, we observed values equal to 68%, 73%, and 78% for NaYF₄:5%Eu-Tyr1, NaYF₄:5%Eu-Tyr2, and NaYF₄:5%Eu-Tyr3, respectively. From the TGA analysis of the particle NaYF₄:5%Eu-Tyr3, obtained after the

three stages of preparation, we found a $\Delta_{\text{Residue}} = 20\%$ of organic compound in its constitution, corroborating with the hypothesis of success in the conjugation process (Fig. 5b). Analogously, compounds NaYF₄:5%Eu-BODIPY COOH (Fig. 5c), NaYF₄:5%Eu-BODIPY NCS (Fig. 5d), and NaYF₄:5%Eu-ZnPc (Fig. 5e) were analyzed using TGA curves, presenting Δ_{Residues} = 23%, 16%, and 9%, respectively. Finally, the particles based in the combination of BODIPY NCS and tyrosine (NaYF4:5%Eu-BODIPY NCS/Tyr3) were also analyzed by TGA, and the compound presented the mass residue equal to $\Delta_{\text{Residue}} = 9\%$ for (Fig. 5f). A more detailed analysis of the $\Delta_{Residue}$ values revealed the ratio of the amount of phenolic compound conjugated to the size of its chemical structure. We observed that less bulky structures, such as Coumaric acid, have a greater residual mass ($\Delta_{\text{Residue}} = 33\%$) in relation to the other compounds, such as BODIPY NCS ($\Delta_{\text{Residue}} = 9\%$). We believe that the steric effect has a significant influence on the conjugation reactions, and consequently, on the increase in residual mass. We also observed that the compounds with ZnPC (Δ Residue = 16%) and BODIPY COOH (\triangle Residue = 23%) present high residual mass, which was related to the greater distance of the molecular mass fraction and the group participating in

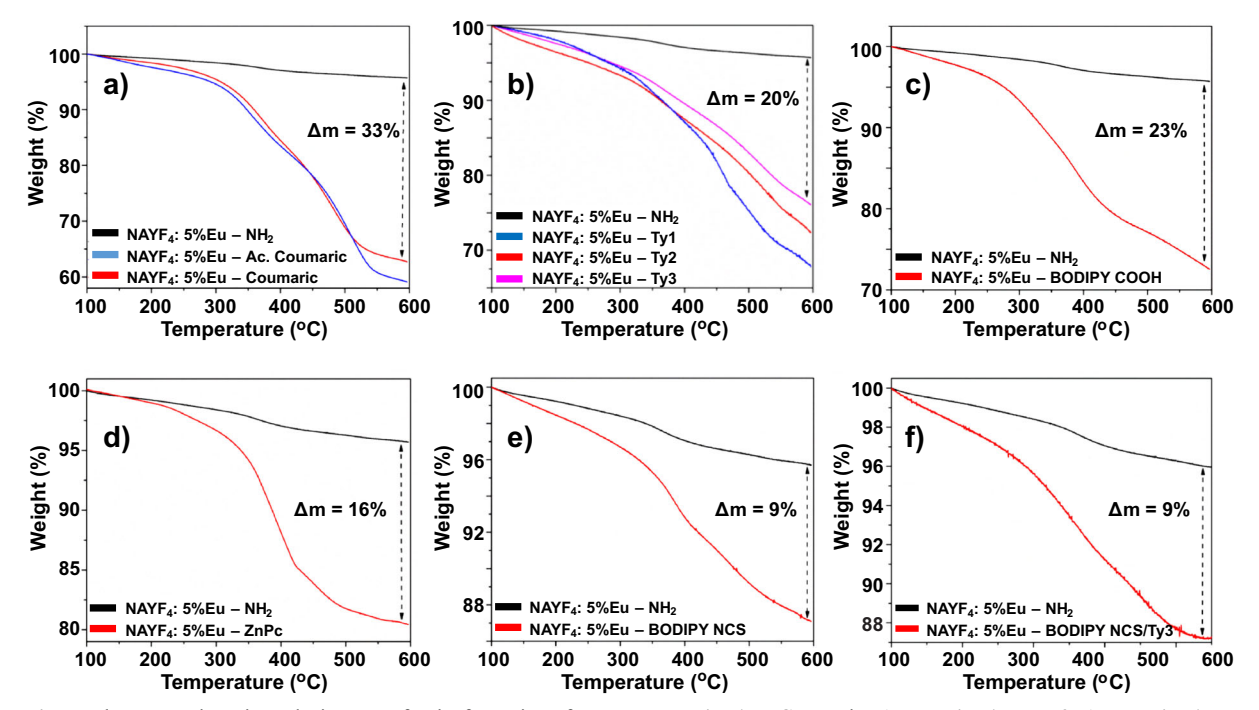


Fig. 5 Thermogravimetric analysis curves for the formation of LNPs a NaYF4:5%Eu-Coumaric, b) NaYF4:5%Eu-Tyr3, c) NaYF4:5%Eu-BODIPY COOH, d) NaYF4:5%Eu-ZnPc, e) NaYF4:5%Eu-BODIPY NCS, and f) NaYF4:5%Eu-BODIPY NCS/Tyr3



23 Page 10 of 15 J Nanopart Res (2019) 21: 23

the coupling reaction, favoring the conjugation. Likewise, tyrosine was also influenced by the steric effect since its initial structure Fmoc-Tyr (tBu) -OH has a considerable volume.

Spectroscopic properties

The optical properties of the compounds were analyzed using excitation and emission spectra where the first results to be presented are the comparison between NaYF₄:5%Eu-NH₂ (Fig. 6a, black line), NaYF₄:5%Eu-Coumaric (Fig. 6a, red line), and NaYF₄:5%Eu-Tyr3 (Fig. 6a, blue line) compounds. Excitation spectra were obtained by monitoring using $\lambda_{\rm Em}$ = 615 nm (Fig. 6a, dotted lines). We observed the compounds presented the characteristic transitions of the Eu³⁺ ion in the inorganic particles $^7F_0 \rightarrow ^5D_4$, 5G_J , 5L_6 , 5D_2 , and 5D_1 (Binnemans 2015). We noticed that the conjugation process with organic molecules did not produce alterations in relation to the compound NaYF₄:5%Eu-NH₂. Emission spectra for NaYF₄:5%Eu-NH₂, NaYF₄:5%Eu-Coumaric, and

NaYF₄:5%Eu-Tyr3 were also obtained by excitation of the $^{7}F_{0} \rightarrow ^{5}L_{6}$ transition ($\lambda_{\rm Ex}$ = 395 nm; full lines). The data in Fig. 5b shows the transitions $^{5}D_{1} \rightarrow ^{7}F_{1,2}$, $^{5}D_{0} \rightarrow ^{7}F_{J}$ (where, J = 0, 1, 2, 3, and 4) that are typical for the trivalent Europium ion, where the $^{5}D_{0} \rightarrow ^{7}F_{2}$ transition is the one with the highest intensity in the spectrum and is also responsible for the characteristic red emission color of the material. The presence of the $^{5}D_{0} \rightarrow ^{7}F_{0}$ transition was also observed that indicates that the metallic center has no inversion center, suggesting that the symmetry site around the ion must have symmetry groups C_{1} , C_{n} , C_{nv} , C_{s} or different arrangements that distortions that lead to these groups (Blasse and Grabmaier 1994; Binnemans 2015; Pathak et al. 2018).

For the luminescence of the compounds NaYF₄:5%Eu-BODIPY COOH (Fig. 5b), NaYF₄:5%Eu-BODIPY NCS (Fig. 6c), NaYF₄:5%Eu-ZnPc (Fig. 6d), and NaYF₄:5%Eu-BODIPY NCS/Tyr3 (Fig. 6e) were analyzed. The excitation spectrum analysis, monitoring the wavelength $\lambda_{\rm Em}=615$ nm, for the compound NaYF₄:5%Eu-BODIPY COOH presented two broad

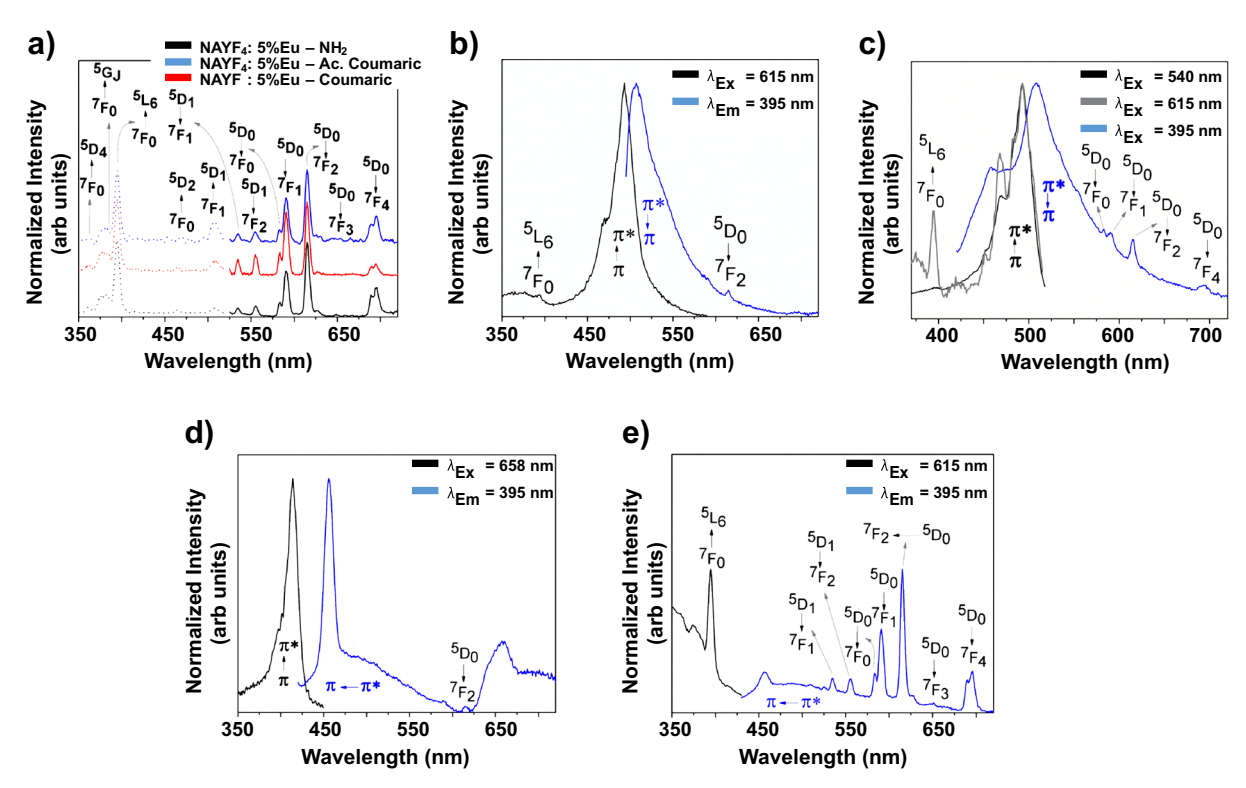


Fig. 6 Excitation and emission spectra for **a)** NaYF₄:5%Eu-NH₂ (black line), NaYF₄:5%Eu-Coumaric (red line), and NaYF₄:5%Eu-Tyr3 (blue line), **b)** NaYF₄:5%Eu-BODIPY COOH (using $\lambda_{em} = 615$ nm and $\lambda_{ex} = 395$ nm), **c)** NaYF₄:5%Eu-BODIPY NCS (using $\lambda_{em} = 615$ nm and $\lambda_{ex} = 395$ nm), **d)**

NaYF₄:5%Eu-ZnPc (using λ_{em} = 658 nm and λ_{ex} = 395 nm), and e) NaYF₄:5%Eu-BODIPY NCS/Tyr3 (using λ_{em} = 615 nm and λ_{ex} = 395 nm) obtained at the concentration of 100 µg/mL in PBS (pH = 7)



bands in the region between 350 and 580 nm, with a maximum centered at 370 nm and 493 nm referring the $\pi \to \pi^*$ transitions of BODIPY COOH conjugated to the particle. It was also possible to observe the transition $^7F_0 \to ^5L_6$ centered at 395 nm, indicating the verification of one of the Eu³+ transitions, occurring to a lesser extent in the synthesized material (Fig. 5b, black line). The emission spectra of NaYF₄:5%Eu-BODIPY COOH, obtained using $\lambda_{\rm Ex}$ = 395 nm, showed a wide band in the region between 500 and 700 nm indicating the relaxation of the $\pi \leftarrow *\pi$ type excited state for the NaYF₄:5%Eu-BODIPY COOH with a maximum centered at 508 nm. In addition, the $^5D_0 \to ^7F_2$ transition was seen in its emission spectrum with lower intensity compared to the emission of the organic part (Fig. 5b, blue line).

The optical behavior of NaYF₄:5%Eu-BODIPY NCS was also studied as shown in Fig. 6c. First, the excitation spectrum for the compound was obtained by monitoring the wavelength $\lambda_{\rm Em}$ = 615 nm (gray line). We can observe a broad band in the region between 325 and 575 nm with centered maxims 467 nm and 493 nm referring to

the transitions $\pi \rightarrow \pi^*$ of the derivative derived from BODIPY NCS and a signal centered at 395 nm referring to the transition ${}^{7}F_{0} \rightarrow {}^{5}L_{6}$ of the Europium ion. In addition, we obtained the excitation spectrum by monitoring the wavelength equal to $\lambda_{\rm Em}$ = 540 nm (black line), which presented the same spectrum obtained in the previous one, with the exception of the transition $^{7}\text{F}_{0} \rightarrow ^{5}\text{L}_{6}$. The emission spectrum of NaYF₄:5%Eu-BODIPY NCS was obtained using the wavelength $\lambda_{\rm Ex}$ = 395 nm, as shown in Fig. 6c (blue line). The emission spectrum is presented in the region between 425 and 720 nm. We observed the presence of the bandwidth with a maximum centered 507 nm resulting from the relaxation $\pi \leftarrow *\pi$ of the conjugated compound. In addition, it is possible to observe emission lines of Eu^{3+ 5}D₀ \rightarrow ⁷F_J ion (where, J = 0, 1, 2, and 4).

Optical behavior was also evaluated for the NaYF₄:5%Eu-ZnPc compounds as shown in Fig. 6d. The excitation spectrum of the compound was obtained by monitoring the wavelength equal to $\lambda_{\rm Em}$ = 658 nm showing a signal centered at 414 nm representing the

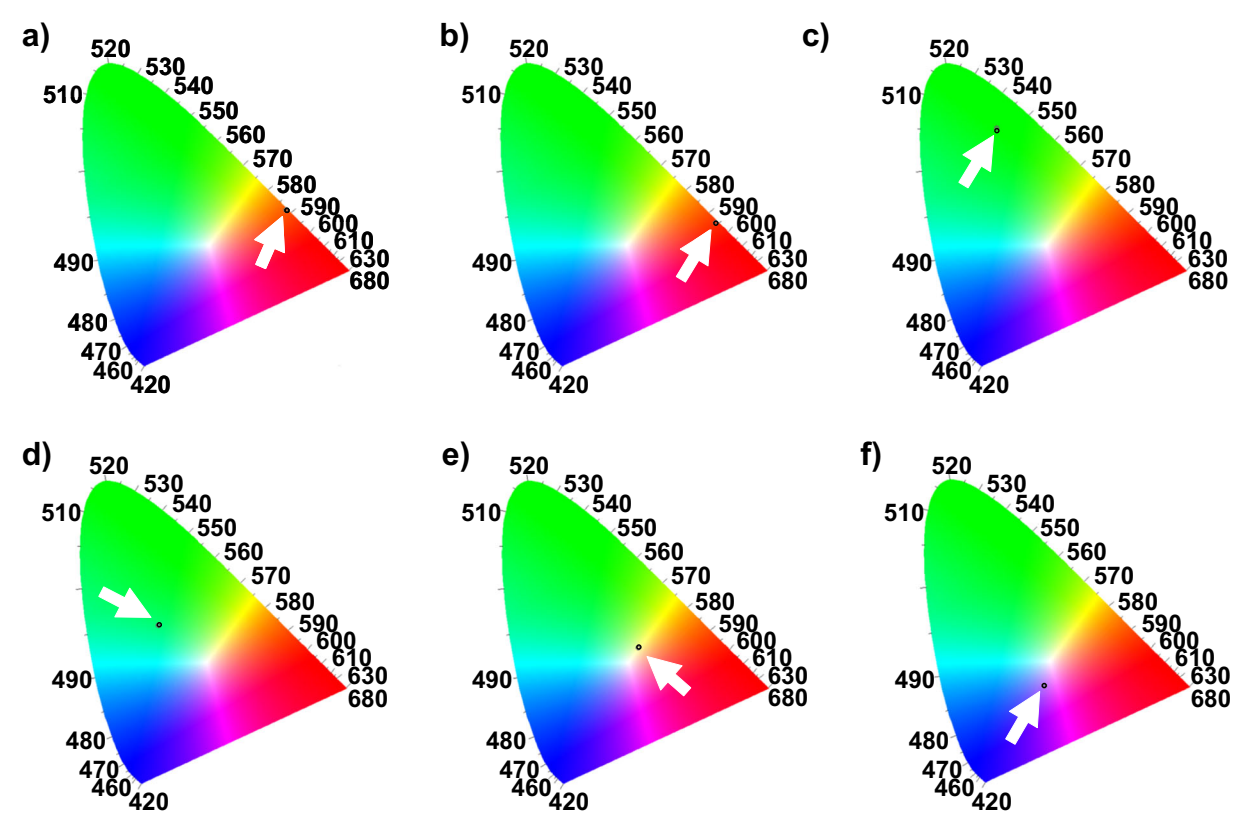


Fig. 7 Color coordinates in the CIE chromaticity diagram for a) NaYF₄:5%Eu-Coumaric, b) NaYF₄:5%Eu-Tyr3, c) NaYF₄:5%Eu-BODIPY COOH, d) NaYF₄:5%Eu-ZnPc, e) NaYF₄:5%Eu-BODIPY NCS, and f) NaYF₄:5%Eu-BODIPY NCS/Tyr3



23 Page 12 of 15 J Nanopart Res (2019) 21: 23

 $\pi \to \pi^*$ transition of the organic part of the conjugate compound (Fig. 6d; black line). The emission spectrum using $\lambda_{\rm Ex}$ = 395 nm showed two signals with maximums at 455 nm and 658 nm relating to relaxation of the ZnPc derivatives in the final conjugate compound. In addition, the compound exhibited a signal of low intensity related to the ${}^5D_0 \to {}^7F_2$ transition relative to the transition of the Eu³⁺ ion in the particles.

The optical behavior for the hybrid compound NaYF₄:5%Eu-BODIPY NCS/Tyr3 was analyzed, as shown in Fig. 5e. For this material, the signal for the Europium ${}^{7}F_{0} \rightarrow {}^{5}L_{6}$ ion at 395 nm was much higher in the emission spectrum when we monitored the wavelength $\lambda_{\rm Em} = 658$ nm (Fig. 6e; black line). The emission spectrum obtained using $\lambda_{\rm Ex} = 395$ nm showed a broad band in the region of 525–675 nm relative to the conjugated BODIPY NCS. We also observed the transitions ff of ion Eu³⁺⁵D₁ \rightarrow ${}^{7}F_{1,2}$ and ${}^{5}D_{0} \rightarrow$ ${}^{7}F_{J}$ (where, J = 0, 1, 2, 3, and 4), as shown in Fig. 5e (blue line).

The CIE (Commission Internationale de L'éclairage [International Commission on Illumination])

chromaticity) diagram is a 2-coordinate system used to represent the color perceived by the human eye from spectroscopic data (Smith and Guild 1931). In the case of the emission spectra presented in Fig. 5, the data could be translated into color coordinates on a CIE chromaticity diagram. As shown in Fig. 7, the LNPs chromaticity diagrams exhibited a different color emission upon irradiating the material with ultraviolet light. The analysis of the CIE chromaticity diagram revealed for NaYF₄:5%Eu-Coumaric a red color and coordinate equal to (0.559; 0.430), for NaYF₄:5%Eu-Tyr3 a red color and coordinate equal to (0.591; 0.596), for NaYF₄:5%Eu-BODIPY COOH a green color and coordinate equal to (0.214; 0.653), for NaYF₄:5%Eu-BODIPY NCS a green color and coordinate equal to (0.218; 0.436), for NaYF₄:5%Eu-BODIPY NCS/Tyr3 a white color and coordinate equal to (0.377; 0.375), and for NaYF₄:5%Eu-ZnPc a pink color and coordinate equal to (0.334; 0.267). These results indicate that the addition of organic chromophore compounds in addition to expanding the light emission range in the

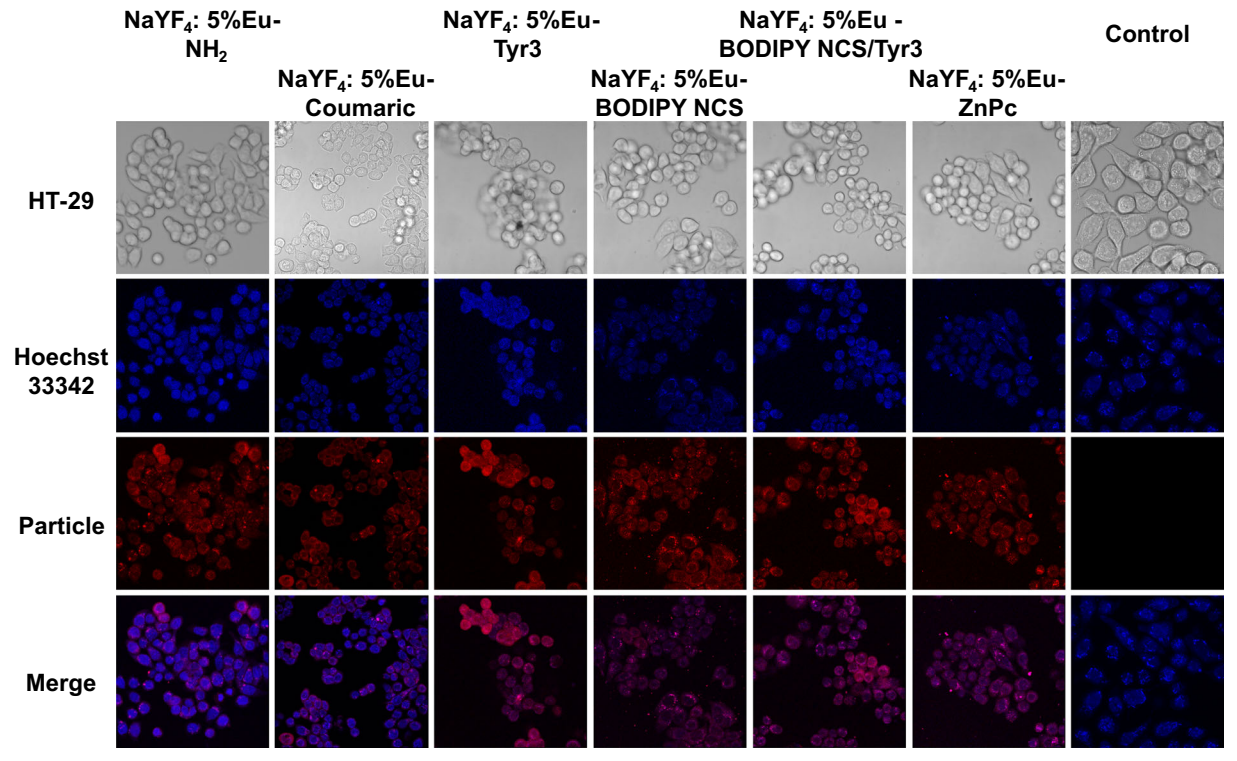


Fig. 8 Confocal microscopy images (× 63 magnified lens) for NaYF₄:5%Eu-NH₂, NaYF₄:5%Eu-Coumaric, NaYF₄:5%Eu-Tyr3, NaYF₄:5%Eu-BODIPY NCS, NaYF₄:5%Eu-BODIPY NCS/Tyr3, and NaYF₄:5%Eu-ZnPc labeled HT-29 cell lines

compared to control (unlabeled) cells. The Hoechst 33342 stained nuclei are shown in blue and the LNP labeled cells are shown in red (excitation and detection at 395 and 500–700 nm, respectively) obtained using a concentration of 100 µg/mL in PBS (pH 7.4)



spectrum modified the resulting color of the LNPs, enabling the color tuning for the desired utilization.

Fluorescence microscopy imaging of the HT-29 cell line

The LNPs: NaYF₄:5%Eu-NH₂, NaYF₄NaYF₄:5%Eu-Coumaric, NaYF₄:5%Eu-Tyr3, NaYF₄:5%Eu-BODIPY NCS, NaYF₄:5%Eu-ZnPc, and NaYF₄:5%Eu-BODIPY NCS/Tyr3 were analyzed using confocal microscopy experiments (Fig. 8). In a preliminary investigation, we observed that the compounds showed uptake into HT-29 cells, with no indication of morphological changes after a 24-h exposure. In addition, the cytotoxicity of NaYF₄:5%Eu-NH₂ was tested on HT-29 cells using an XTT assay to assess the biocompatibility of the precursor particles. The assays performed reveal that cellular viability was not significantly affected by nanoparticles at concentrations of 1, 10, and 100 µg/mL (Fig. S15). These data show satisfactory results that the material can serve as a promising nanoprobe with low cytotoxicity. Likewise, BODIPY, ZnPc, p-Coumaric acid, and Tyrosine compounds are widely reported in the literature as having nontoxic cellular interactions, in the form of biomarkers (Loudet and Burgess 2007; Escobedo et al. 2010; Naskar et al. 2016; Bizet et al. 2018) or as molecular constituents present in foods (Soobrattee et al. 2005; Pandey and Rizvi 2009; Dziedzic et al. 2018), supporting their use in the context of the NaYF4:5%Eu nanoparticles.

After the conjugation procedure, the NaYF₄:5%Eu-Tyr3, NaYF₄:5%Eu-BODIPY NCS, NaYF₄:5%Eu-ZnPc, and NaYF₄:5%Eu-BODIPY NCS/Tyr3 nanoparticles showed excellent cellular affinity, represented by the accumulation of luminescent particles on the surface of HT-29 cells. A more detailed analysis shows that even with the difference in the emitted light intensities, all LNPs had cellular absorption deposited into the cytoplasm region. In the literature, we found some other particulate markers that show similarity in the interaction in the cytoplasm region, supporting the obtained results (Wolfbeis 2015; Yan et al. 2015). These data show that the synthesized materials are promising for imaging composition and bioassays by exploiting their luminescence properties. However, the luminescent images showed that the NaYF₄:5%Eu-NH₂ compound lacked good affinity for HT-29 cells, suggesting that additional surface modifications may be necessary to increase this property. In addition, we did not notice any significant changes in cellular luminescence after exposure to NaYF₄:5%-Coumaric nanoparticles, suggesting that this material was not efficient for our application.

Conclusions

The synthesis of the six new LNPs: NaYF₄:5%Eu-Coumaric, NaYF₄:5%Eu-Tyr3, NaYF₄:5%Eu-BODIPY COOH, NaYF4:5%Eu-BODIPY NCS, NaYF4:5%Eu-BODIPY NCS/Tyr3, and NaYF₄:5%Eu-ZnPc was performed by coupling reactions, mostly using an amidification methodology with TBTU as the coupling agent and combining NaYF₄:5%Eu-NH₂ particles and acid donor compounds. The results of the PXRD analysis indicated the formation of particles NaYF₄:5%Eu and NaYF₄:5%Eu-NH₂ both organized in the crystalline phase of β-NaYF₄ in the space group P-6 with hexagonal symmetry obtained with high phase purity. TEM analyses revealed the formation of nanoparticles smaller than 50 nm. Detailed investigation of the fingerprinted region in the FT-IR spectra indicated the formation of the conjugated particles. From the thermal analysis, it was possible to quantify the organic moiety covalently bound to the particles, showing that there was conjugation in all synthesized materials. The optical properties of NaYF4:5%Eu-Coumaric and NaYF4:5%Eu-Tyr3 showed only the f-f transitions of the 4f⁶ configuration of the Eu³⁺ ion for excitation and emission spectra. On the other hand, the compounds NaYF₄:5%Eu-BODIPY COOH, NaYF4:5%Eu-BODIPY NCS, NaYF4:5%Eu-BODIPY NCS/Tyr3, and NaYF₄:5%Eu-ZnPc presented wide bands in the excitation and emission spectra, which were related to the conjugated organic chromophores on the surface of the particles. In addition, these compounds also presented the Eu3+ transitions with lower intensity. The evaluation of LNPs as targeting colon cancer cells was performed; we observed that the compounds showed cellular internalization with no morphological damage to HT-29 cells after 24 h. These results revealed the promising character of LNPs for application in medical devices for cancer detection.

Acknowledgments The authors thank the staff in the Department of Chemistry, the Department of Comparative Biomedical Sciences, and the Shared Instrument Facility at Louisiana State University (USA), and the Fundamental Chemistry Department at the Federal University of Pernambuco (Brazil) for their technical support. We gratefully acknowledge the CNPq (Conselho Nacional de Desenvolvimento Científico e Tecnológico), FACEPE (Fundação de Amparo à Ciência e Tecnologia do Estado



de Pernambuco), CAPES (Coordenação de Aperfeiçoamento de Pessoal de Nível Superior), and the NSF (National Science Foundation) for funding in support of this work.

Funding This work was jointly supported by Brazil grants from the FACEPE (grant nos. APQ-0742-1.06/15, APQ-0675-1.06/14, APQ-0549-1.06/17) and from the CNPq (grant no. 428020/2016-0). We also acknowledge the FACEPE for a Brazilian scholarship (grant no. IBPG-1414-3.03/14) and CAPES for an international scholarship through the Science without Borders program (88887.122971/2016-00). USA funding was supported through the NSF (grant no. 1800126) and provided by the LSU School of Veterinary Medicine. These funders had no role in study design, data collection and analysis, decision to publish, or preparation and submission of the manuscript.

Compliance with ethical standards

Conflict of interest The authors declare that they have no conflict of interest.

Publisher's Note Springer Nature remains neutral with regard to jurisdictional claims in published maps and institutional affiliations.

References

- Ansari AA, Yadav R, Rai SB (2016) A facile synthesis approach and impact of shell formation on morphological structure and luminescent properties of aqueous dispersible NaGdF₄:Yb/Er upconversion nanorods. J Nanopart Res 18:. https://doi. org/10.1007/s11051-016-3622-8
- Arnold M, Sierra MS, Laversanne M, Soerjomataram I, Jemal A, Bray F (2017) Global patterns and trends in colorectal cancer incidence and mortality. Gut 66:683–691. https://doi.org/10.1136/gutjnl-2015-310912
- Bhunia SK, Saha A, Maity AR, Ray SC, Jana NR (2013) Carbon nanoparticle-based fluorescent bioimaging probes. Sci Rep 3. https://doi.org/10.1038/srep01473
- Binnemans K (2015) Interpretation of europium(III) spectra. Coord Chem Rev 295:1–45. https://doi.org/10.1016/j.ccr.2015.02.015
- Bizet F, Ipuy M, Bernhard Y, Lioret V, Winckler P, Goze C, Perrier-Cornet JM, Decréau RA (2018) Cellular imaging using BODIPY-, pyrene- and phthalocyanine-based conjugates. Bioorganic Med Chem 26:413–420. https://doi. org/10.1016/j.bmc.2017.11.050
- Blasse G, Grabmaier BC (1994) Luminescent materials. SpringerVerlag
- Bor G, Üçüncü M, Emrullahoğlu M, Tomak A, Şanlı-Mohamed G (2017) BODIPY-conjugated chitosan nanoparticles as a fluorescent probe. Drug Chem Toxicol 40:375–382. https://doi.org/10.1080/01480545.2016.1238481
- Bünzli J-CG, Piguet C (2005) Taking advantage of luminescent lanthanide ions. Chem Soc Rev 34:1048–1077. https://doi. org/10.1039/b406082m

- Barbosa CDES, Corrêa JR, Medeiros GA, Barreto G, Magalhães KG, de Oliveira AL, Spencer J, Rodrigues MO, Neto BAD (2015) Carbon dots (C-dots) from cow manure with impressive subcellular selectivity tuned by simple chemical modification. Chem A Eur J 21:5055–5060. https://doi.org/10.1002/chem.201406330
- Dziedzic K, Górecka D, Szwengiel A, Olejnik A, Rychlik J, Kreft I, Drożdżyńska A, Walkowiak J (2018) The cytotoxic effect of artificially digested buckwheat products on HT-29 colon cancer cells. J Cereal Sci 83:68–73. https://doi.org/10.1016/j.jcs.2018.07.020
- Escobedo JO, Rusin O, Lim S, Strongin RM (2010) NIR dyes for bioimaging applications. Curr Opin Chem Biol 14:64–70. https://doi.org/10.1016/j.cbpa.2009.10.022
- Generalova AN, Chichkov BN, Khaydukov EV (2017) Multicomponent nanocrystals with anti-stokes luminescence as contrast agents for modern imaging techniques. Adv Colloid Interf Sci 245:1–19. https://doi.org/10.1016/j. cis.2017.05.006
- Hildebrandt N, Spillmann CM, Algar WR, Pons T, Stewart MH, Oh E, Susumu K, Díaz SA, Delehanty JB, Medintz IL (2017) Energy transfer with semiconductor quantum dot bioconjugates: a versatile platform for biosensing, energy harvesting, and other developing applications. Chem Rev 117:536–711. https://doi.org/10.1021/acs.chemrev.6b00030
- Johnson NJJ, Oakden W, Stanisz GJ, Scott Prosser R, van Veggel FCJM (2011) Size-tunable, ultrasmall NaGdF₄ nanoparticles: insights into their T₁ MRI contrast enhancement. Chem Mater 23:3714–3722. https://doi.org/10.1021/cm201297x
- Karakoti AS, Shukla R, Shanker R, Singh S (2015) Surface functionalization of quantum dots for biological applications. Adv Colloid Interf Sci 215:28–45. https://doi.org/10.1016/j. cis.2014.11.004
- Kim HM, Cho BR (2015) Small-molecule two-photon probes for bioimaging applications. Chem Rev 115:5014–5055. https://doi.org/10.1021/cr5004425
- Kostiv U, Janoušková O, Šlouf M, Kotov N, Engstová H, Smolková K, Ježek P, Horák D (2015) Silica-modified monodisperse hexagonal lanthanide nanocrystals: synthesis and biological properties. Nanoscale 7:18096–18104. https://doi.org/10.1039/C5NR05572E
- Li J, Chang X, Chen X, Gu Z, Zhao F, Chai Z, Zhao Y (2014) Toxicity of inorganic nanomaterials in biomedical imaging. Biotechnol Adv 32:727–743. https://doi.org/10.1016/j. biotechadv.2013.12.009
- Liu M, Ye Y, Yao C, Zhao W, Huang X (2014) Mn²⁺-doped NaYF₄:Yb/Er upconversion nanoparticles with amplified electrogenerated chemiluminescence for tumor biomarker detection. J Mater Chem B 2:6626–6633. https://doi. org/10.1039/C4TB00717D
- Loudet A, Burgess K (2007) BODIPY dyes and their derivatives: syntheses and spectroscopic properties. Chem Rev 107: 4891–4932. https://doi.org/10.1021/cr078381n
- Luo PG, Sahu S, Yang S-T, Sonkar SK, Wang J, Wang H, LeCroy GE, Cao L, Sun YP (2013) Carbon "quantum" dots for optical bioimaging. J Mater Chem B 1:2116. https://doi.org/10.1039/c3tb00018d
- Naskar B, Modak R, Sikdar Y, Maiti DK, Banik A, Dangar TK, Mukhopadhyay S, Mandal D, Goswami S (2016) A simple Schiff base molecular logic gate for detection of Zn²⁺ in water and its bio-imaging application in plant system. J



- Photochem Photobiol A Chem 321:99–109. https://doi.org/10.1016/j.jphotochem.2016.01.022
- Oluwole DO, Uddin I, Prinsloo E, Nyokong T (2016) The effects of silica based nanoparticles on the photophysicochemical properties, in vitro dark viability and photodynamic therapy study of zinc monocarboxyphenoxy phthalocyanine. J Photochem Photobiol A Chem 329:221–231. https://doi.org/10.1016/j.jphotochem.2016.07.002
- Pandey KB, Rizvi SI (2009) Plant polyphenols as dietary antioxidants in human health and disease. Oxidative Med Cell Longev 2:270–278. https://doi.org/10.4161/oxim.2.5.9498
- Pathak TK, Kumar A, Swart HC, Kroon RE (2018) Effect of annealing on structural and luminescence properties of Eu³⁺ doped NaYF₄ phosphor. Physica B: Condensed Matter 535: 132–137. https://doi.org/10.1016/j.physb.2017.06.086
- Scudiero DA, Shoemaker RH, Paull KD, Monks A, Tierney S, Nofziger TH, Currens SD, Boyd MR (1988) Evaluation of a soluble tetrazolium/formazan assay for cell growth and drug sensitivity in culture using human and other tumor cell lines. Cancer Res 48:4827–4833
- Siegel RL, Miller KD, Fedewa SA, et al (2017) Colorectal Cancer Statistics, 2017. CA Cancer J Clin 67:177–193. https://doi. org/10.3322/caac.21395
- Smith T, Guild J (1931) The C.I.E. colorimetric standards and their use. Trans Opt Soc 33:73–134. https://doi.org/10.1088/1475-4878/33/3/301
- Sojka B, Podhorodecki A, Banski M, Misiewicz J, Drobczynski S, Dumych T, Lutsyk MM, Lutsyk A, Bilyy R (2016) β-NaGdF₄:Eu³⁺ nanocrystal markers for melanoma tumor imaging. RSC Adv 6:57854–57862. https://doi.org/10.1039/C6 RA10351K
- Soobrattee MA, Neergheen VS, Luximon-Ramma A, Aruoma OI, Bahorun T (2005) Phenolics as potential antioxidant therapeutic agents: mechanism and actions. Mutat Res Mol Mech Mutagen 579:200–213. https://doi.org/10.1016/j. mrfmmm.2005.03.023
- Stöber W, Fink A, Bohn E (1968) Controlled growth of monodisperse silica spheres in the micron size range. J Colloid Interface Sci 26:62–69. https://doi.org/10.1016/0021-9797 (68)90272-5

- Syamchand SS, George S (2016) The upconversion luminescence and magnetism in Yb³+/Ho³+ co-doped LaF3 nanocrystals for potential bimodal imaging. J Nanopart Res 18:385. https://doi.org/10.1007/s11051-016-3699-0
- Tu D, Liu Y, Zhu H, Li R, Liu L, Chen X (2013) Breakdown of crystallographic site symmetry in lanthanide-doped NaYF₄ crystals. Angew Chemie Int Ed 52:1128–1133. https://doi. org/10.1002/anie.201208218
- Valeur E, Bradley M (2009) Amide bond formation: beyond the myth of coupling reagents. Chem Soc Rev 38:606–631. https://doi.org/10.1039/B701677H
- Veber DF, Johnson SR, Cheng H et al (2002) Molecular properties that influence the oral bioavailability of drug candidates. J Med Chem 45:2615–2623. https://doi.org/10.1021/jm020017n
- Wang K, Zhuang J, Liu Y, Xu M, Zhuang J, Chen Z, Wei Y, Zhang Y (2018) PEGylated chitosan nanoparticles with embedded bismuth sulfide for dual-wavelength fluorescent imaging and photothermal therapy. Carbohydr Polym 184:445–452. https://doi.org/10.1016/j.carbpol.2018.01.005
- Waring MJ (2010) Lipophilicity in drug discovery. Expert Opin Drug Discov 5:235–248. https://doi.org/10.1517/17460441003605098
- Wolfbeis OS (2015) An overview of nanoparticles commonly used in fluorescent bioimaging. Chem Soc Rev 44:4743–4768. https://doi.org/10.1039/C4CS00392F
- Xu X, Zhang X, Wu Y (2016) Folic acid-conjugated GdPO₄: Tb³⁺@ SiO₂ nanoprobe for folate receptor-targeted optical and magnetic resonance bi-modal imaging. J Nanoparticle Res. https://doi.org/10.1007/s11051-016-3649-x
- Yan J, He W, Li N, Yu M, du Y, Lei B, Ma PX (2015) Simultaneously targeted imaging cytoplasm and nucleus in living cell by biomolecules capped ultra-small GdOF nanocrystals. Biomaterials 59:21–29. https://doi.org/10.1016/j.biomaterials.2015.04.041
- Zhou JC, Yang ZL, Dong W, Tang RJ, Sun LD, Yan CH (2011)
 Bioimaging and toxicity assessments of near-infrared upconversion luminescent NaYF₄:Yb, Tm nanocrystals.
 Biomaterials 32:9059–9067. https://doi.org/10.1016/j.biomaterials.2011.08.038

